Preparation and application of magnetite nanoparticles immobilized on cellulose acetate nanofibers for lead removal from polluted water

Thanaa I. Shalaby, Marwa F. El-Kady, Abd El Halem M. Zaki and Soheir M. El-Kholy

ABSTRACT

Novel magnetic cellulose acetate (CA) nanofibers were fabricated using an electrospinning process. Co-precipitated magnetite iron oxide nanoparticles were immobilized onto CA nanofibers at different weight ratios (0.2–2.5% wt/v) with a CA concentration of 15% (wt %), applied electric voltage of 20 kV, feeding rate of 1.5 ml/h and 7 cm distance between needle tip and collector. The prepared iron oxide nanoparticles were characterized using X-ray diffraction, a transmission electron microscope, a Fourier transform infrared spectrophotometer (FT-IR) and a vibrating sample magnetometer (VSM). The magnetic nanofibers were characterized by scanning electron microscopy, FT-IR, thermogravimetric analysis and VSM. The fabricated composite nanofibers were evaluated as a sorbent matrix for lead decontamination from aqueous solution using a batch technique. The influence of solution pH, contact time and adsorbent concentration on the removal efficiency was investigated. Adsorption kinetics models and isotherms were applied to the lead decontamination process onto the fabricated composite nanofibers. The kinetics of the sorption process revealed that the pseudo-second-order model fitted relatively better than the pseudo-first-order model. On the other hand, both the Langmuir and Freundlich isotherms gave a comparable fit to the adsorption data, with a high coefficient of regression of 0.999.

Key words | adsorption, cellulose acetate, electrospinning, heavy metals, magnetic nanocomposite

Thanaa I. Shalaby (corresponding author)
Abd El Halem M. Zaki
Soheir M. El-Kholy
Medical Biophysics Department,
Medical Research Institute,
Alexandria,
Egypt
E-mail: *th_shalaby@yahoo.com*

Marwa F. El-Kady
Chemical and Petrochemical Engineering Department,
Egypt-Japan University of Science and Technology,
New Borg El-Arab City,
Alexandria,
Egypt
and
Fabrication Technology Researches Department
Advanced Technology and New Materials Researches Institute,
City of Scientific Research and Technological Applications (SRTA-City),
New Borg El-Arab City,
Alexandria
Egypt

INTRODUCTION

The development of energy-efficient water treatment technology has become an important area of research as it offers a solution to the increasingly limited water supplies available to the world's growing population and industry. Nanotechnology is currently at the forefront of the latest research in water treatment and has been identified as a useful tool in resolving current problems in water treatment. Nanotechnology comprises the fabrication and functionality of materials with dimensions within the nano-scale (1–100 nm). Because of the larger surface area to volume ratio and smaller size, chemical and physical properties of the material are altered, giving it novel qualities (Goyal *et al.* 2011).

Various forms of nanotechnology, such as nanobiocides, nanofibers and nanofiltration, are currently being developed and in some cases used in water treatment for chemical decontamination, desalination, filtration and sanitation. Nanofibers have enormous potential for application in water filtration and sanitation. Due to the small pores in a non-woven mat of electrospun nanofibers, nanofibrous mats have excellent filtration properties, and due to the variety of polymers that can be used to fabricate nanofibers, and the versatility of being able to add functional molecules and chemical groups to the nanofibers, nanofibers are applicable to the sanitation and purification of water (Feng *et al.* 2013). Different approaches to producing nanofibers have been reported, such as drawing, templates, phase separation, self-assembly and electrospinning. Among them, electrospinning is the most convenient, low-cost and high-speed

doi: 10.2166/ws.2016.124

method of producing nanocomposite fibers. Electrospinning is a process that involves applying a high voltage (more than 6 kV) between the tip of a needle and a collecting electrode (collector). A pendant drop of solution under surface tension will be charged, and the induced charges will be evenly distributed over the surface. The Coulomb repulsive force will overcome the solution surface tension and thus force the ejection of a liquid jet, which results in the formation of a Taylor cone. The electrified jet of viscoelastic solution then undergoes a stretching process and forms thin fibers on the collector (Nguyen *et al.* 2011).

The nanofibers produced by electrospinning have several remarkable advantages including: small diameter (50 nm–10 μm), high aspect ratio (the ratio of length to diameter), large specific surface area (surface to volume ratio), diverse composition, unique physicochemical properties, and design flexibility for chemical/physical surface functionalization. Together with the complex pore structure and easy fiber surface modification, electrospun nanofibers are ideal for certain applications (Chronakis 2005; Uyar *et al.* 2009).

Cellulose acetate (CA), a derivative of cellulose, can be easily obtained from natural resources and is recycled in the environment by biodegradation. According to Chronakis (2005), it can be easily fabricated into films, membranes and fibers. CA has been widely used in membranes for separation and medical applications, because of its good hydrolytic stability and relatively low cost.

The association of CA with different fillers can bring benefits like improved properties (optical, mechanical, hardness…) and delivering unique functions by their use. CA has been used as a soft matrix to accommodate inorganic fillers to produce composites that bring together the intrinsic functionalities of the fillers and the bio-interfaces offered by cellulose fibers (Lu & Drzal 2010). A growing interest in the development of electrospun CA as blends and composites has been witnessed in the last few years. The combination of CA and magnetite NPs can be obtained in the nanofibrous form by an electrospinning technique to overcome the problem of aggregation assigned to magnetite NPs as it will be well distributed in the CA matrix and also to give the CA magnetic properties as well as more thermal and mechanical stability.

The aim of this study was to fabricate novel magnetic CA nanofibers. Firstly, the various electrospinning parameters affecting fabrication of the homogenous CA nanofibers was optimized. The optimized CA nanofibers were immobilized with different weights of magnetic iron oxide nanoparticles (0.2–2.5% wt/v) to fabricate various magnetic composite nanofibers. The possibility of utilizing the fabricated magnetic nanofibers as easily separated reusable membranes for lead removal from simulated water was explored.

MATERIALS AND METHODS

Materials

Ferrous chloride tetrahydrate ($FeCl_2.4H_2O \geq 99\%$), ferric chloride hexahydrate ($FeCl_3.6H_2O \geq 99\%$) and sodium hydroxide (NaOH) pellets, CA ($M_n = 50{,}000$, 39.8 wt% acetyl content), N,N-dimethylformamide (DMF) (purity > 98%) and acetone (purity > 98%). All chemicals were purchased from Sigma Aldrich Co., Germany.

Methods

Preparation of magnetite nanoparticles (Fe_3O_4 NPs)

Iron oxide nanoparticles were synthesized using a co-precipitation method (Petcharoen & Sirivat 2012). $FeCl_2.4H_2O$ and $FeCl_3.6H_2O$ [1:2 molar ratio, respectively] were dissolved in about 50 ml deionized water solution and stirred for 10–15 min followed by addition of 1.0 M NaOH solution until the appearance of a black precipitate. To ensure complete growth of the nanoparticle crystals, the reaction was carried out for 30 min at 80 °C under constant stirring and bubbling of N_2 gas. Black Fe_3O_4 NPs were decanted by a permanent magnet and washed with ultrapure water several times and then in ethanol. The particles were finally dried in a vacuum oven at 70 °C.

Fabrication of nano-magnetite immobilized CA nanofibers

A polymer solution of 15% (wt%) CA dissolved in acetone/DMF (2:1) mixed solution was prepared. The mixture was stirred at room temperature for ~3 hours until a clear, transparent solution was obtained. Finally, a specific amount of

magnetite NPs (0–2.5% wt/v) was thoroughly mixed into the polymer solution. Ultra-sonication was applied for 15 min to disperse the Fe_3O_4 nanoparticles in the CA solution at room temperature. The magnetite dispersed solution was immediately collected into a 10 ml syringe equipped with a stainless steel blunted tip needle (inner diameter of 0.7 mm) as an electrode which connected to a direct current (DC) high-voltage generator (Gamma High Voltage Research, Inc., USA). The magnetic CA nanofibers were prepared using the electrospinning technique in an air-conditioned laboratory. The process conditions were kept at an ambient temperature of 22 °C and relative humidity of <65%. The syringe was fixed on an electric syringe pump set to maintain a constant feed rate of 1.5 ml/h. A high voltage power supply (Gamma High Voltage Research, Inc., USA) was employed to apply positive charge to the needle, and a grounded metal plate covered with aluminum foil served as the collector. The voltage used for the electro-spinning process was 20 kV. The distance between the needle tip and collector was 7 cm. Before electrospinning, CA solution viscosity and conductivity were measured using a (Cannon Fenske) viscometer and conductivity meter (Horiba ES-12, Japan) at room temperature, respectively.

Characterization of prepared powder magnetite nanoparticles and composite nanofibers

The size and morphological structure of prepared Fe_3O_4 nanoparticles were determined by transmission electron microscopy (TEM, JEOL-100 CX). Crystallographic structures were investigated using an X-ray diffractometer (Shimadzu, XRD-7000, Maxima, Japan) operated at a voltage of 30 kV and a current of 30 mA with CuKα radiation (=1.54 Å) and analyzed between 5 and 100 ° (2θ). The Fourier transform infrared (FT-IR) spectrum of magnetite was recorded on an FT-IR spectrophotometer (Shimadzu, Japan, FT-IR-8400S), all measurements being carried out in the range of 400–4000 cm^{-1} at a resolution of 4 cm^{-1}. The degree of magnetism of the prepared magnetite was evaluated using a vibrating sample magnetometer (VSM-9600-1DSM-LDG-USA). The hysteresis loops were measured under a magnetic field strength of 20,000 Gauss at room temperature. The data were taken with 80 points/loop with a scan speed of 10 s/point.

With respect to the fabricated nanofiber matrices, the morphology (size, shape and diameter) of the pure CA and CA/Fe_3O_4 composite nanofiber membranes was evaluated using scanning electron microscopy (SEM, JEOL-5300, Japan). FT-IR spectroscopy was used to characterize the electrospun pure CA and CA/Fe_3O_4 composite nanofibers. The magnetic properties of the nanofiber composites at room temperature were evaluated using a VSM. The thermal behavior of the composite nanofibers was examined using thermal gravimetric analysis (Shimadzu, TGA-50, Japan). The experiment was carried out by weighing a powder sample of around 5 mg and loading it into a platinum pan. The mass change under the temperature scan from 25 to 600 °C at a heating rate of 20 °C/min and under a nitrogen flow of 20 ml/min was monitored and recorded.

Batch adsorption techniques for lead decontamination onto magnetic composite nanofibers

A standard stock solution of Pb(II) (1 g/L) was prepared by dissolving pure $Pb(NO_3)_2$. The stock solution was prepared in deionized water and the desired concentrations of metal ions were obtained by dilution using the same water. 0.1 M HNO_3 and 0.1 M NaOH solutions were used for pH adjustment of the synthetic waste solutions. The affinity of the fabricated composite nanofibers for lead sorption was monitored using a batch technique. 0.1 g of CA/Fe_3O_4 composite nanofibers was added to 50 ml solutions of lead simulated wastewater at various initial concentrations (10–100 ppm). The adsorption behavior of composite nanofibers was examined over different contact time intervals (5–180 min) using a shaking incubator. The influence of initial solution pH (2–9) was determined. Samples were withdrawn from the solutions at desired time intervals, and the ion concentration of the solution was determined using an atomic absorption spectrophotometer (Shimadzu AA6300C, Japan). The amount of adsorbed metal ions (q_t, mg/g) on the composite nano-fiber was calculated using the following equations:

$$q_t = \frac{c_0 - c_t}{W} V \quad (1)$$

where c_0 and c_t are the concentrations of metal ions (mg/L) initially and at time t, respectively. V is the volume of the solution (L) and m is the mass of the CA/Fe_3O_4 nanofibers (g).

RESULTS AND DISCUSSION

Characterization of magnetic iron oxide nanoparticles

TEM morphological studies

The TEM micrograph revealed that the synthesized Fe_3O_4 NPs were multi-dispersed spherical nanoparticles with average particles size of 10 ± 3 nm, the extremely small particle size achieving great specific surface area and surface energy. No mono-dispersion of nanoparticles was observed due to the high surface energy of iron oxide nanoparticles in an aqueous medium that tends to form aggregates (Figure 1). The electron diffraction pattern, which is characteristic of the inverse cubic spinel structure of Fe_3O_4, is illustrated in Figure 1.

XRD

The XRD pattern of as-prepared iron oxide is shown in Figure 2. The XRD pattern is indexed as a pure cubic Fe_3O_4 structure compared with the reference (JCPDS Card No. 03–0863). The main characteristic diffraction peaks

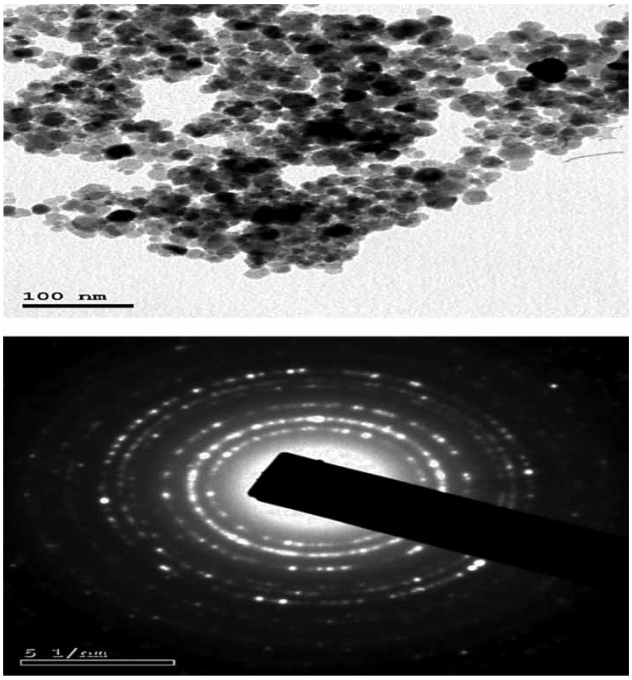

Figure 1 | TEM micrograph and diffraction pattern of Fe_3O_4 NPs.

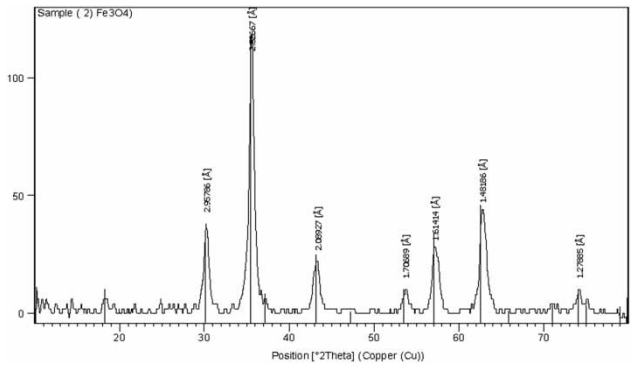

Figure 2 | XRD of bare Fe_3O_4 NPs.

were recorded at $2\theta = 35.48$, 62.62, 30.12, 57.02, and 43.12 and can be assigned to (311), (440), (220), (511) and (400) planes of Fe_3O_4 NPs, respectively (Sun & Zeng 2002). Accordingly, the XRD results confirm that the as-prepared nanoparticles can be identified as magnetite Fe_3O_4.

Fabrication of nano-magnetite immobilized CA nanofibers

CA/Fe_3O_4 composite nanofibers with different Fe_3O_4 nanoparticle loadings (0.2–2.5% wt/v) were fabricated. Fe_3O_4 NP loadings increase the solution viscosity, which prevents a continuous polymer solution jet and subsequent fiber formation. It can be seen from SEM images of CA and CA/Fe_3O_4 NFs (0.2–2.5 wt%) that the Fe_3O_4 NPs are well dispersed in the polymer matrix and the spinning conditions were successfully optimized to obtain smooth bead-free fibers. It is clear from Figure 3(a)–3(g) that as the concentration of Fe_3O_4 NPs increased, the fabricated nanofiber diameter decreased. However, CA/Fe_3O_4 NFs with magnetite concentrations higher than 1% (wt/v) exhibit no further significant decrease in fiber diameter. These results can be explained by the competitive effects of increasing magnetite concentrations and the corresponding increase in conductivity and viscosity of the polymer solutions, as can be seen from Table 1. These results were confirmed by previous studies (Deitzel *et al.* 2001; Huang *et al.* 2003) which showed that an increase in fiber diameter is obtained by increasing the electrospun solution viscosity and a decrease in fiber diameter is observed by increasing the solution conductivity. Accordingly, these two effects seem to cancel

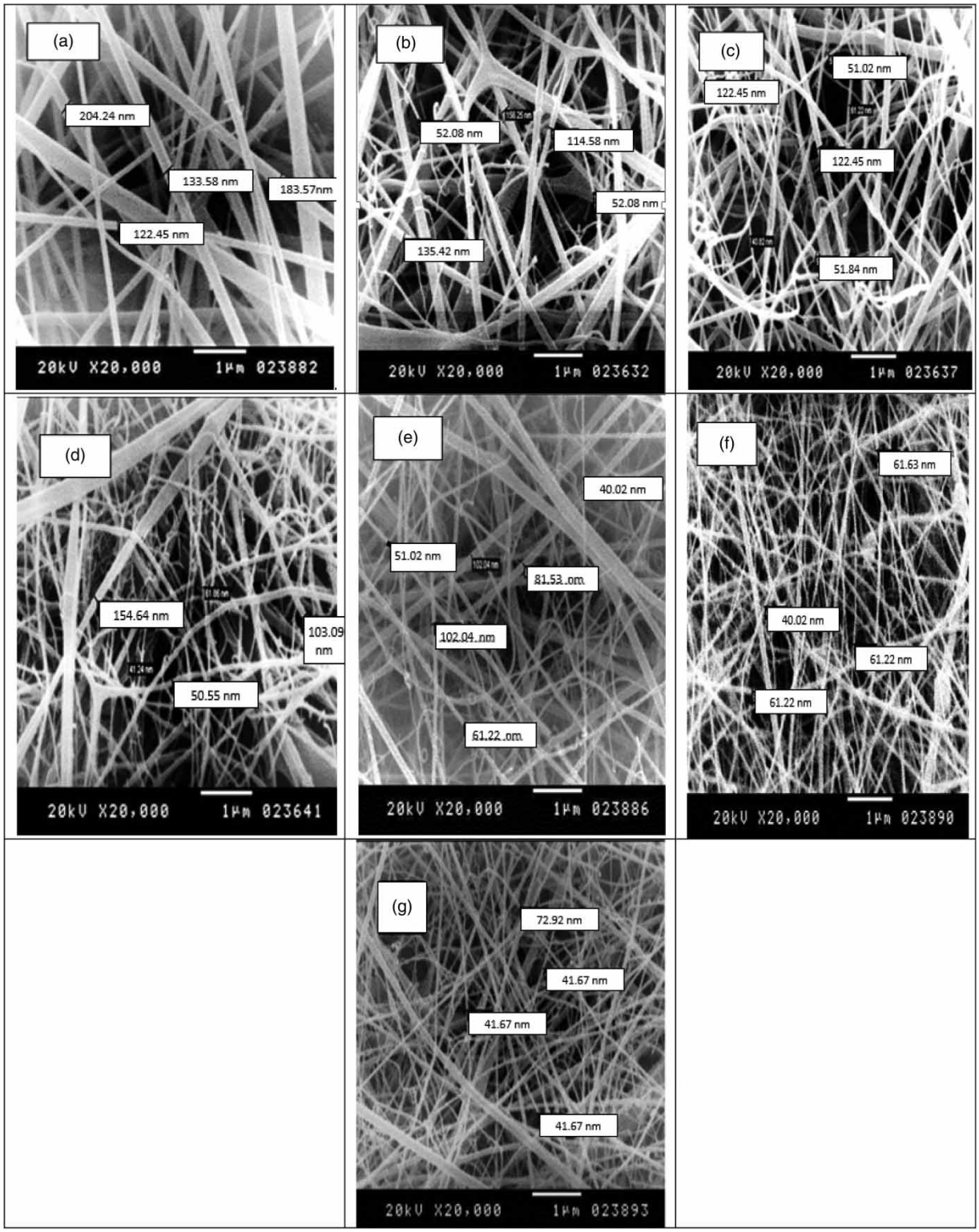

Figure 3 | SEM images of CA/Fe_3O_4 (0, 0.2, 0.5, 1.0, 1.5, 2.0 and 2.5 wt/v) composite NFs: (a)–(g) respectively.

Table 1 | Conductivity and viscosity values of CA and CA/Fe_3O_4 polymeric solutions

Solution	Conductivity (μS/cm)	Viscosity (mPa.s)
CA (11 wt%)	4.8	404.9
CA (13 wt%)	8.6	629.5
CA (15 wt%)	11.5	1048.0
CA/Fe_3O_4 (0.2% wt/v)	13.3	1054.6
CA/Fe_3O_4 (0.5% wt/v)	27.1	16,861.1
CA/Fe_3O_4 (1% wt/v)	35.8	1856.2
CA/Fe_3O_4 (1.5% wt/v)	44.5	1181.3
CA/Fe_3O_4 (2% wt/v)	47.1	2332.9
CA/Fe_3O_4 (2.5% wt/v)	47.9	2387.7

each other out, with no great influence of the iron oxide content on the fiber size. Moreover, it was also observed that the viscosity value of CA/Fe_3O_4 (1.5% wt/v) substantially dropped, to 1181.3 (mPa.s), which is lower than the CA viscosity value itself. This result was also found by Tsioptsias and it was attributed to the hindrance of interaction between polymer molecules by Fe_3O_4 NPs (Tsioptsias *et al.* 2010).

Characterization of fabricated nano-magnetite immobilized CA nanofibers

TGA

In order to identify the influence of the presence of magnetite nanoparticles on the CA nanofibers, the TGA of both CA and CA composite nanofibers were compared. The thermogram curves of pure CA and CA/Fe_3O_4 NFs were compared and investigated as shown in Figure 4. Both thermograms showed the initial weight loss at temperatures below 200 °C refers to the evaporation of adsorbed water and any solvent residuals. While CA NFs showed 81.18% weight loss in three-step thermal decomposition range starting from 243 °C and ending at 462 °C. However, CA/Fe_3O_4 NFs showed 86.899% weight loss in a three-step thermal decomposition range starting from 280 °C and ending at 599 °C. This result elucidates the positive effect of adding magnetite NPs to CA NFs as it delays the starting point of decomposition from 243 °C to 280 °C as well as widening the major decomposition window from 291 °C to 319 °C. Adsorption of polymer chains on the surface of nanostructures results in restriction of segmental mobility and serves to suppress redistribution and chain transfer reactions. Also, Fe_3O_4 NPs have a barrier effect, slowing down mass transport (volatilization) and thermal transport during decomposition of the polymer (Jalajerdi *et al.* 2012).

FT-IR

FT-IR analysis was performed to reveal the surface nature of Fe_3O_4, CA and CA/Fe_3O_4 (2.5% wt/v) as shown in Figure 5. Infrared spectrums at low wavenumbers (≤700 cm^{-1}) were obtained from vibrations of Fe–O bonds. Additional peaks at 1625 and 3337 cm^{-1} can be attributed to the vibrational modes of the hydroxyl groups on the surface of the magnetite nanoparticles or the residual water molecules in the sample (Sun & Zeng 2002).

Comparing this spectrum with FT-IR spectroscopy of CA and CA/Fe_3O_4 (2.5% wt/v), an absorption peak occurs at 1750 cm^{-1} that is related to the C=O bond in CA. Absorptions at 1383 and 1434 cm^{-1} are attributed to C–CH_3

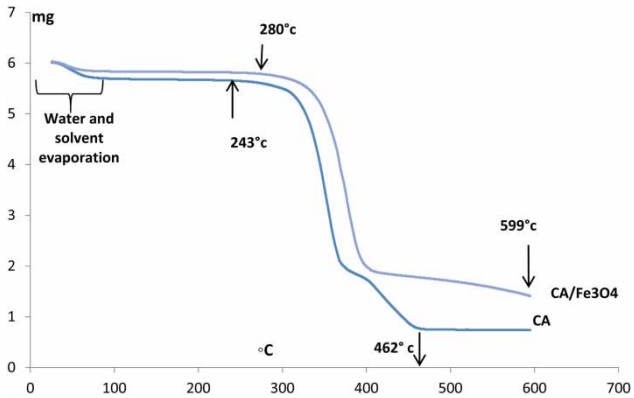

Figure 4 | Thermograms of CA NFs (a) and CA/Fe_3O_4 (2.5% wt/v) NFs (b).

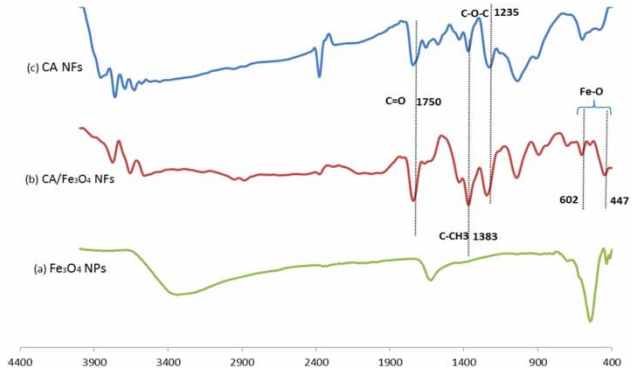

Figure 5 | FT-IR spectrum of Fe_3O_4 NPs (a), CA/Fe_3O_4 (2.5% wt/v) nanocomposite fibers (b) and CA nanofibers (c).

symmetric and asymmetric vibrations in CA polymer. Absorptions at 1235 cm^{-1} are attributed to C–O–C. Also, the absorptions at 3487 cm^{-1} are referred to the stretching vibration of O–H bond. The peaks around 1000 cm^{-1} may be attributed to DMF remnants resulting from incomplete evaporation. The absorption at 447 and 600 cm^{-1} for nanocomposites confirms the existence of Fe_3O_4 nanoparticles in the polymeric matrix (Khan & Singh 2010).

VSM

Magnetic properties are strongly influenced by many parameters, including crystallinity, size, shape and crystal defects. Room temperature magnetic properties of our samples were studied using a VSM device. Hysteresis loops for Fe_3O_4 nanoparticles and CA/Fe_3O_4 (2.5% wt/v) composite nanofibers are depicted in Figure 6. The hysteresis loops of the magnetic nanoparticles and composite nanofibers show superparamagnetic behavior. Clearly, the saturation magnetization (M_s) of Fe_3O_4 nanoparticles (48.4507 emu/g at 19.1047 kG) is much higher than that obtained for CA/Fe_3O_4 nanocomposite fibers (2.284 emu/g at 19.1047 kG). The hysteresis loops show that the remanence and the coercivity are close to zero (Jalajerdi *et al.* 2012).

Batch technique for lead decontamination using magnetic CA nanofibers

A batch experiment was conducted to determine the efficacy of the prepared composite nanofiber membrane to remove heavy metals from contaminated water; the experiment was conducted to remove Pb(II) from simulated water.

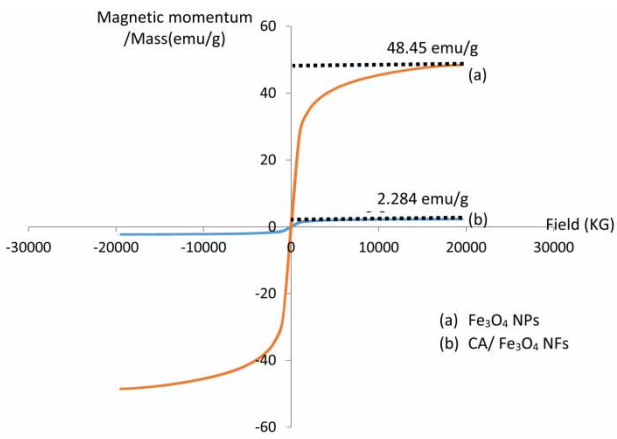

Figure 6 | VSM graphs of Fe_3O_4 NPs (a) and CA/Fe_3O_4 NFs (2.5% wt/v) (b).

Effect of contact time and initial concentration

The schemes for the removal of Pb(II) from aqueous solution using CA/Fe_3O_4 (2.5% wt/v) composite nanofibers as adsorbents with varying both contact time and initial concentration are shown in Figures 7 and 8, respectively. The effects of contact time on the adsorption process were studied in the time range from 0 to 180 min at pH = 6 and 27 °C with a fixed adsorbent dose (0.1 g/50 ml). It was observed that the lead adsorption increased with increasing contact time. The adsorption increased rapidly during the first 30 min, and then it was moderate up to 50 min, while after 60 min the adsorption remained constant.

There are two steps in the adsorption of lead metal ions. In the initial step, adsorption was swift because of the large

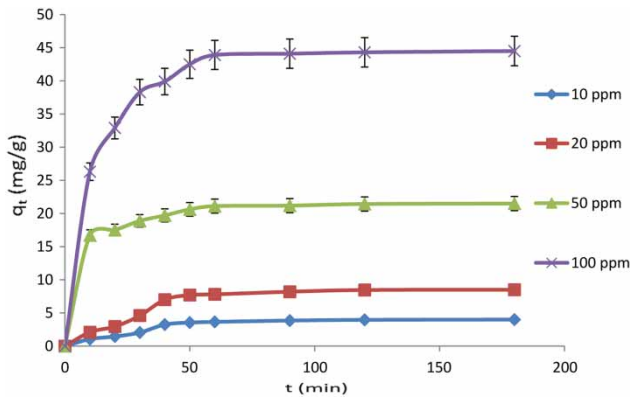

Figure 7 | Adsorption of Pb(II) on 0.1 g CA/Fe_3O_4 NFs (2.5% wt/v) in 50 ml solution with different initial concentrations at pH = 6 and 27 °C.

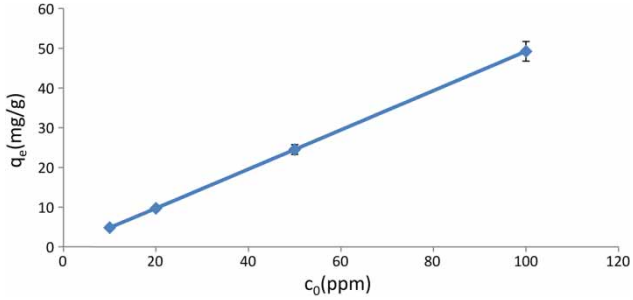

Figure 8 | The dependence of the equilibrium adsorption capacity of Pb(II) ions on the initial concentrations.

number of free adsorptive sites and the high concentration of the metal. In the second step, adsorption rates decreased. This was a direct effect of the depletion of the adsorptive sites as well as the decrease in the metal ion concentration in the testing solutions.

Figure 8 illustrates that the increase in the amount of lead ions adsorbed at equilibrium (q_e) from 5 to 50 mg/g with the corresponding increment in initial lead concentration from 10 to 100 ppm. This behavior can be explained by the increase in the ion diffusion driving force.

Effects of pH

pH is one of the most important parameters controlling the removal of heavy metals from waste water. The adsorption of Pb(II) onto both CA and CA/Fe_3O_4 composite nanofibers as a function of solution pH is presented in Figure 9. The maximum removal efficiency of CA/Fe_3O_4 composite nanofibers for Pb(II) was 98.4%, recorded at a pH value of 7. Pure CA fiber was also examined for the removal of metal ions under the same conditions. As a result, the CA/Fe_3O_4 composite nanofiber exhibited significantly higher removal capacities of metal ions than the pure CA nanofiber. Therefore, the adsorption of metal ions was mostly attributed to the Fe_3O_4 nanoparticles in the CA/Fe_3O_4 composite nanofiber.

It is clear from the results that pH has a momentous role on adsorption of metals using the prepared membrane. It was found that increasing the pH of the solution from 2 to 6 increases the percentage removal of metal (from 47.2% to 98.4%).

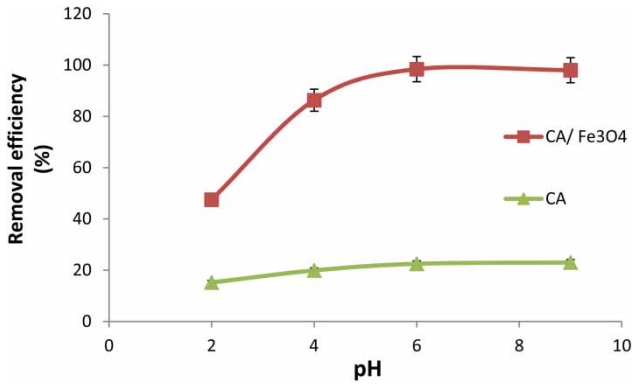

Figure 9 | Effect of pH on Pb(II) removal efficiency by the CA nanofibers and the CA/Fe_3O_4 composite nanofibers. Reaction conditions: initial metal ion concentration 50 mg/L; adsorbent amount 0.1 g/50 ml; adsorption time 24 h; and temperature 27 °C.

It can be easily seen that the adsorption capacity for both CA and CA/Fe_3O_4 composite nanofibers in weak acidic or neutral solution was better than that in strong acidic solution. The increase in Pb(II) ion removal with pH is due to the decline in competition between the protons and Pb(II) ion species for surface sites beside decreasing the Coulomb repulsion that occurs between the protonated surface and Pb(II) ion species at low pH. It was also reported that pH values higher than 7 may affect the adsorption studies by facilitating Pb(II) ion precipitation to lead hydroxides (Khan & Singh 2010).

Adsorption kinetics of lead ions onto composite nanofibers

The adsorption kinetics data were fitted to pseudo-first-order (PFO), pseudo-second-order (PSO) and the intraparticle diffusion models to investigate the adsorption mechanisms.

The PFO model is expressed by S. Lagergren's equation as:

$$\log(q_e - q_t) = \log q_e - K_1 t \tag{2}$$

where q_e and q_t (mg/g) are the amount of metal ions adsorbed on a magnetic membrane at equilibrium and at time t, respectively. K_1 (min^{-1}) is the rate constant of the PFO adsorption (Lagergren 1898).

The PSO model is expressed by the equation of Ho and McKay as:

$$\frac{t}{q_t} = \frac{1}{K_2 q_e^2} + \frac{t}{q_e} \tag{3}$$

where K_2 ($g\,mg^{-1}\,min^{-1}$) is the rate constant of the PSO adsorption (Ho & McKay 1999).

The intra-particle diffusion model (IDM) proposed by Weber and Morris can be expressed as follows:

$$q_t = K_{id}\sqrt{t} + C \tag{4}$$

where K_{id} is the intra-particle diffusion rate constant (mg/g $min^{1/2}$); C is the intercept (mg/g) that gives information

about the thickness of the boundary layer. If the plot of q_t versus $t_{1/2}$ is linear and passes through the origin then intra-particle diffusion is the sole rate-limiting step but if the plot of q_t versus $t_{1/2}$ is not linear over the entire time range, then the intra-particle transport is not the only rate-limiting step in the adsorption process and consequently, the adsorption is also affected by boundary layer diffusion (Ma *et al.* 2007).

Figures 10–12 show the fitting of adsorption kinetics data of Pb(II) on 0.1 g CA/Fe_3O_4 NFs (2.5% wt/v) in 50 ml solution at pH = 6 and 27 °C to PFO, PSO and IDMs, respectively. The three models' parameters are tabulated in Table 2.

It can be seen that the adsorption kinetics data are well fitted to both the PFO and PSO models, with high correlation values (R^2) averaging 0.92 and 0.99, respectively. χ^2 values were calculated for PFO and PSO models to compare the fitting qualities of adsorption kinetics data to them based

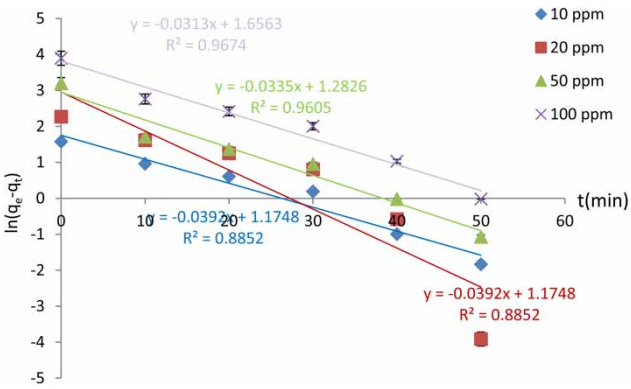

Figure 10 | PFO plot of Pb(II) adsorption on 0.1 g CA/Fe_3O_4 NFs (2.5% wt/v) in 50 ml solution at pH = 6 and 27 °C.

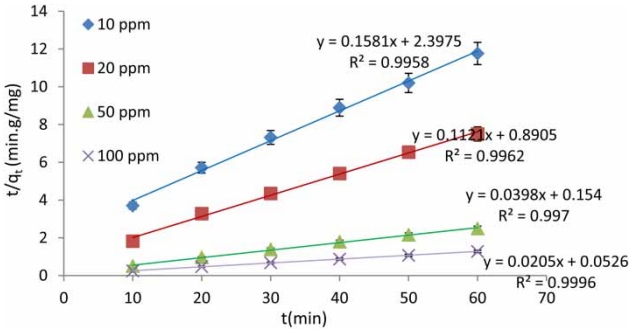

Figure 11 | PSO plot of Pb(II) adsorption on 0.1 g CA/Fe_3O_4 NFs (2.5% wt/v) in 50 ml solution at pH = 6 and 27 °C.

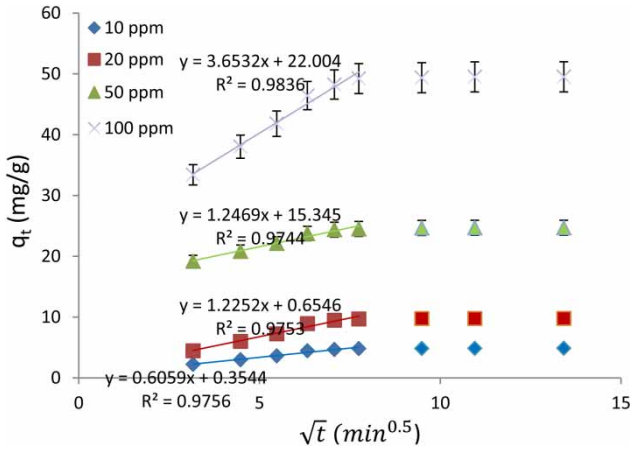

Figure 12 | Intra-particle diffusion plot of Pb(II) adsorption on 0.1 g CA/Fe_3O_4 NFs (2.5% wt/v) in 50 ml solution at pH = 6 and 27 °C.

Table 2 | Kinetic parameters calculated from different kinetic models for the adsorption of Pb(II) on CA/Fe_3O_4 (2.5% wt/v) NFs

	Pb(II)			
Model	**10 ppm**	**20 ppm**	**50 ppm**	**100 ppm**
PFO				
R^2	0.8852	0.8852	0.9605	0.9674
$q_{e\ model}$ (mg/g)	3.2374	3.1953	3.6060	5.2398
$q_{e\ experimental}$ (mg/g)	5.1	8	24.1	47.01
χ^2		457.750		
K_1 (min^{-1})	0.0392	0.0349	0.0335	0.0313
PSO				
R^2	0.9958	0.9962	0.997	0.9996
$q_{e\ model}$ (mg/g)	6.3251	8.9206	25.1256	48.7804
$q_{e\ experimental}$ (mg/g)	5.1	8	24.1	47.01
χ^2		0.4384		
K_2 (g mg^{-1} min^{-1})	0.0249	0.0125	0.0015	0.0004
Intra-particle diffusion				
R^2	0.9756	0.9753	0.9744	0.9836
K_{id} (mg/g $min^{1/2}$)	0.6059	1.2252	1.2469	3.6532

on the following equation:

$$\chi^2 = \sum \frac{(Q_{e\ experimental} - Q_{e\ model})^2}{Q_{e\ model}} \quad (5)$$

where $q_{e\ experimental}$ is the value of q_e determined from the experiment and $q_{e\ model}$ is the value of q_e calculated from the intercepts of the best fitted linear equations that represent the PFO and PSO models (Nassar 2010).

It is obvious from Table 2 that the χ^2 value for PSO is much smaller than that of PFO, which means that PSO is more efficient in predicting the adsorption mechanism. This finding accompanies the close matching between $q_{e\ experimental}$ and $q_{e\ model}$ values for PSO model.

The IDM confirmed that the adsorption process is dependent on the intra-particle transport in addition to the boundary layer diffusion.

Adsorption isotherms

Analysis of adsorption isotherms is of fundamental importance to describe how adsorbate molecules interact with the adsorbent surface. The Freundlich isotherm was employed to describe heterogeneous systems and reversible adsorption, which is not restricted to monolayer formations. Unlike the Freundlich isotherm, the Langmuir isotherm is based on the assumption that the structure of the adsorbent is homogeneous, where all sorption sites are identical and energetically equivalent.

The Langmuir isotherm is expressed as follows:

$$\frac{c_e}{q_e} = \frac{1}{q_m K_l} + \frac{c_e}{q_m} \quad (6)$$

where q_e (mg/g) is the equilibrium metal ion concentration on the adsorbent, c_e (mg/L) is the equilibrium metal ion concentration in solution, q_m (mg/g) is the monolayer capacity of the adsorbent and K_l (L/mg) is the Langmuir adsorption coefficient.

The fundamental characteristics of the Langmuir equation can be interpreted in terms of a dimensionless constant separation factor (R_L), which is defined by

$$R_L = \frac{1}{1 + K_l c_0} \quad (7)$$

where K_l (L/mg) is the Langmuir constant related to the energy of adsorption and c_0 (mg/L) is the lowest initial concentration. The value of R_l could indicate the shape of the isotherm to be either unfavorable ($R_L > 1$) or linear ($R_L = 1$) or favorable ($0 < R_L < 1$) or irreversible ($R_L = 0$) (Liu 2006).

The Freundlich adsorption isotherm can be expressed as:

$$\log q_e = \log K_f + \frac{1}{n} \log c_e \quad (8)$$

where q_e (mg/g) is the equilibrium metal ion concentration on the adsorbent, and c_e (mg/L) is the equilibrium metal ion concentration in solution. K_f ((mg/g) (mg/L)$^{-1/n}$) and n are the Freundlich coefficients that can be related to the adsorption capacity and the adsorption intensity, respectively (Quiñones & Guiochon 1996).

Figures 13 and 14 represent the plots of the experimental data and the fitted Langmuir and Freundlich isotherm equations, respectively. Table 3 shows the calculated values of the Langmuir and Freundlich isotherm coefficients.

Examination of the correlation coefficients reported in the study shows that the Langmuir and Freundlich isotherms are applicable to interpreting lead adsorption on the composite nanofibrous membrane.

As the lead adsorption process obeys both Langmuir and Freundlich isotherms, we could propose the adsorption to be a chemical sorption between Pb(II) and the acetate group in

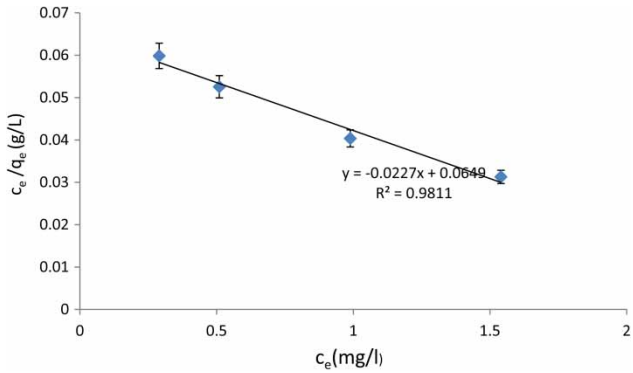

Figure 13 | Langmuir isotherm for the adsorption of Pb(II) on the CA/Fe_3O_4 (2.5% wt/v) NFs.

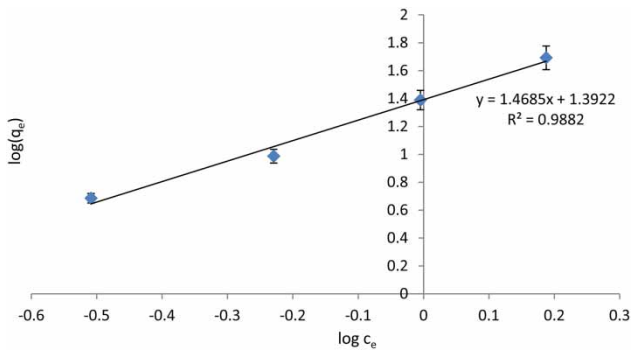

Figure 14 | Freundlich isotherm for the adsorption of Pb(II) on the CA/Fe_3O_4 (2.5% wt/v) NFs.

Table 3 | Adsorption isothermal coefficients calculated from Langmuir and Freundlich isotherms

Isotherms	Pb(II)
Langmuir	
R^2	0.9811
q_m (mg/g)	44.0528
K_l (L/mg)	0.3497
R_L	0.9079
Freundlich	
R^2	0.9882
K_f ((mg/g) $(mg/L)^{-1/n}$)	24.6717
N	0.6809

CA and also physical adsorption between the negative surface charge of amphoteric Fe_3O_4 NPs and positive ions of Pb(II). Accordingly the lead adsorption process onto CA/Fe_3O_4 nanofibers is a mainly physicochemical process.

The R_L constant has a value of 0.9079, which means that the adsorption process of lead ions on the CA/Fe_3O_4 NF membrane is a favorable process, i.e. it does not need an external energy to happen.

CONCLUSION

This investigation succeeded in incorporating the coprecipitated Fe_3O_4 NPs into a CA matrix to fabricate CA/Fe_3O_4 NP composite nanofibers. The fabrication of composite nanofibers with different amounts of Fe_3O_4 NPs was optimized and monitored using SEM. The optimized CA nanofibers were immobilized with different weights of magnetic iron oxide nanoparticles (0.2–2.5% wt/v) to fabricate various magnetic composite nanofibers. The incorporation of iron oxide nanoparticles into the CA polymer enhanced the thermal stability and magnetization of CA. The applicability of CA/Fe_3O_4 NP composite nanofibers for lead ion decontamination was tested over various processing conditions. The incorporation of nanomagnetite into CA improved its lead sorption capacity compared with pure CA nanofibers. The increase in both the initial lead concentration and solution pH had a positive effect on the lead adsorption process onto the composite nanofibers. A PSO model and the Freundlich isotherm described the lead adsorption kinetics and isotherm data on composite nanofibers well, suggesting the physicochemical nature of the adsorption process.

ACKNOWLEDGEMENTS

The authors acknowledge financial support from the Science & Technology Development Fund in Egypt (STDF) Project No. 5821 'Removal of Heavy Metals from El-Salam Canal by Adsorption on some Sinai Natural Product in Conjugation with Nanomaterials'.

REFERENCES

Chronakis, I. S. 2005 Novel nanocomposites and nanoceramics based on polymer nanofibers using electrospinning process – a review. *Journal of Materials Processing Technology* **167** (2), 283–293. DOI: 10.1016/j.jmatprotec.2005.06.053

Deitzel, J., Kleinmeyer, J., Harris, D. & Tan, N. B. 2001 The effect of processing variables on the morphology of electrospun nanofibers and textiles. *Polymer* **42** (1), 261–272. DOI: 10.1016/S0032-3861(00)00250-0.

Feng, C., Khulbe, K. C., Matsuura, T., Tabe, S. & Ismail, A. F. 2013 Preparation and characterization of electro-spun nanofiber membranes and their possible applications in water treatment. *Separation and Purification Technology* **102**, 118–135. DOI: 10.1016/j.seppur.2012.09.037

Goyal, K. A., Johal, S. E. & Rath, G. 2011 Nanotechnology for water treatment. *Current Nanoscience* **7** (4), 640–654. DOI: 10.2174/157341311796196772.

Ho, Y. S. & McKay, G. 1999 Pseudo-second order model for sorption processes. *Process Biochemistry* **34** (5), 451–465. DOI: 10.1016/S0032-9592(98)00112-5.

Huang, Z. M., Zhang, Y. Z., Kotaki, M. & Ramakrishna, S. 2003 A review on polymer nanofibers by electrospinning and their applications in nanocomposites. *Composites Science and Technology* **63** (15), 2223–2253. DOI: 10.1016/S0266-3538(03)00178-7.

Jalajerdi, R., Gholamian, F., Shafie, H., Moraveji, A. & Ghanbari, D. 2012 Thermal and magnetic characteristics of cellulose acetate-Fe_3O_4. *Journal of NanoStructures* **1** (2), 105–109.

Khan, T. A. & Singh, V. V. 2010 Removal of cadmium (II), lead (II), and chromium (VI) ions from aqueous solution using clay. *Toxicological and Environmental Chemistry* **92** (8), 1435–1446. DOI: 10.1080/02772241003592930.

Lagergren, S. 1898 About the theory of so-called adsorption of soluble substances. *Kungliga Svenska Vetenskapsakademiens Handlingar* **24** (4), 1–39.

Liu, Y. 2006 Some consideration on the Langmuir isotherm equation. *Colloids and Surfaces A: Physicochemical and Engineering Aspects* **274** (1), 34–36. DOI: 10.1016/j.colsurfa.2005.08.029.

Lu, J. & Drzal, L. T. 2010 Microfibrillated cellulose/cellulose acetate composites: effect of surface treatment. *Journal of Polymer Science Part B: Polymer Physics* **48** (2), 153–161. DOI: 10.1002/polb.21875.

Ma, W., Ya, F. Q., Han, M. & Wang, R. 2007 Characteristics of equilibrium, kinetics studies for adsorption of fluoride on magnetic-chitosan particle. *Journal of Hazardous Materials* **143** (1), 296–302. DOI: 10.1016/j.jhazmat.2006.09.032.

Nassar, N. N. 2010 Rapid removal and recovery of Pb (II) from wastewater by magnetic nanoadsorbents. *Journal of Hazardous Materials* **184** (1), 538–546. DOI:10.1016/j.jhazmat.2010.08.069.

Nguyen, T. T. T., Tae, B. & Park, J. S. 2011 Synthesis and characterization of nanofiber webs of chitosan/poly (vinyl alcohol) blends incorporated with silver nanoparticles. *Journal of Materials Science* **46** (20), 6528–6537. DOI: 10.1007/s10853-011-5599-0.

Petcharoen, K. & Sirivat, A. 2012 Synthesis and characterization of magnetite nanoparticles via the chemical co-precipitation method. *Materials Science and Engineering: B* **177** (5), 421–427. DOI: 10.1016/j.mseb.2012.01.003.

Quiñones, I. & Guiochon, G. 1996 Derivation and application of a Jovanovic–Freundlich isotherm model for single-component adsorption on heterogeneous surfaces. *Journal of Colloid and Interface Science* **183** (1), 57–67. DOI:10.1006/jcis.1996.0518.

Sun, S. & Zeng, H. 2002 Size-controlled synthesis of magnetite nanoparticles. *Journal of the American Chemical Society* **124** (28), 8204–8205. DOI: 10.1021/ja026501x.

Tsioptsias, C., Sakellariou, K. G., Tsivintzelis, I., Papadopoulou, L. & Panayiotou, C. 2010 Preparation and characterization of cellulose acetate–Fe_2O_3 composite nanofibrous materials. *Carbohydrate Polymers* **81** (4), 925–930. DOI: 10.1016/j.carbpol.2010.04.005.

Uyar, T., Nur, Y., Hacaloglu, J. & Besenbacher, F. 2009 Electrospinning of functional poly (methyl methacrylate) nanofibers containing cyclodextrin-menthol inclusion complexes. *Nanotechnology* **20** (12), 125703. DOI: 10.1088/0957-4484/20/12/125703.

First received 21 March 2016; accepted in revised form 19 July 2016. Available online 27 July 2016